Computerized Optimal Control System Design for Boost Vehicles

WOLFGANG TRAUTWEIN*
Lockheed Missiles & Space Company Inc., Huntsville, Ala.
AND
JOHN M. LIVINGSTON†
NASA Marshall Space Flight Center, Huntsville, Ala.

An optimization technique has been developed which combines the practical features of hybrid simulation of the dynamic systems with the systematic approach of modern control theory. Standard hybrid computer optimization methods using high-speed repetitive simulations and gradient minimization schemes have been extended to obtain time-varying optimal gain schedules and reduce the sensitivity of the optimized system to parameter and disturbance uncertainties. In this approach the performance index is expressed in meaningful engineering terms that reflect the interactions among all major design disciplines. The basic optimization technique is developed and its application to the space shuttle is presented. Control gain schedules, vehicle design and performance characteristics resulting from the technique are compared with controllers developed by conventional methods.

Introduction

A WELL-designed attitude control system for space shuttle ascent can significantly contribute to the economy of this new transportation system. Best use should be made of all available control forces from thrust vector control (TVC) and from aerodynamic surface deflections to stabilize the vehicle and control its ascent trajectory. The wide range of possible control and blending schemes and their mostly conflicting impact on vehicle design and performance make a systematic design approach highly desirable.

The overriding design criterion in all booster control problems should be to stabilize the vehicle while the orbital insertion weight is maximized. Such a payload maximization criterion combines all the standard design criteria (load relief, minimum drift, etc.) in the most meaningful manner and provides the key to a computerized optimal design approach to solve the following problem. For a given boost vehicle, determine time-varying attitude control gain schedules (and schedules for blending TVC and aerodynamic control in the case of winged vehicles) so that orbit insertion weight is maximized.

Problem Formulation

Let the dynamics of the system (plant) be described by

$$\dot{\bar{x}} = \bar{f}(\bar{x}, \bar{u}, t) \tag{1}$$

where $\bar{x}$ is the n-dimensional state vector, $\bar{f}$ an n-dimensional functional vector, $\bar{u}$ an m-dimensional control vector ($m \leq n$) and $(\cdot) = d/dt$.

For this discussion we assume a linear control law and performance measure to be minimized as follows:

$$\bar{u}(t) = K(t)\,\bar{x}(t) \tag{2}$$

$$J = J(\bar{x}, \bar{u}, t) \tag{3}$$

where K is an $m \times n$ gain matrix.

In the search for a practical solution technique which reduces the computational load, quadratic optimal control theory was closely examined. To this end the system Eqs. (1) were linearized to the following form:

$$\dot{\bar{x}} = F(t)\bar{x} + G(t)\beta + H(t)\alpha_w \tag{4}$$

where F, G, H are time-varying coefficient matrices, β is the thrust vector deflection angle and α_w is the external time-varying scalar forcing function (wind angle of attack).

A quadratic performance criterion was formulated[1] which reduces bending loads $M_B = M_\alpha\alpha + B_\beta\beta$ and maintains acceptable trajectory performance: (prime denotes transpose)

$$J = \tfrac{1}{2}\int_0^T \left(\bar{x}'Q\bar{x} + \frac{M_B{}^2}{M_\beta{}^2}\right)dt \tag{5}$$

Then the system is optimal if its control law minimizes J over the total atmospheric flight phase for a suitably chosen weighting matrix Q.

Standard Quadratic Control Theory Solution

Applying linear optimal control theory, the optimal control law can be shown to be

$$\beta^\circ(t) = K(t)\bar{x}(t) - k(t)\alpha_w(t) + G'(t)\bar{\zeta}(t) \tag{6}$$

where $k(t) = M_\alpha/M_\beta$.

$$K(t) = -G'P(t) - k(t)\bar{a}' \tag{7}$$

is the optimal time-varying feedback gain row vector and $\bar{a}$ is a constant vector.

The $n \times n$ matrix P is the solution of the set of Riccati differential equations

$$-\dot{P} = P\tilde{F} + \tilde{F}P - PGG'P + Q \tag{8}$$

and the vector $\bar{\zeta}$ is the solution of the differential equation

$$\dot{\bar{\zeta}} = -(\tilde{F} - GG'P)'\bar{\zeta} + P(H - kG)\alpha_w \tag{9}$$

Presented as Paper 72-98 at the AIAA 10th Aerospace Sciences Meeting, San Diego, Calif., January 17-19, 1972; submitted February 4, 1972; revision received November 10, 1972. The authors wish to acknowledge the contributions of C. J. Chang, C. L. Connor, and K. R. Leimbach in the control system study and of A. M. Hansing in the hybrid programing and computing.

Index categories: Launch Vehicle and Controlled Missile Dynamics and Control; Navigation, Control, and Guidance Theory; Launch Vehicle and Missile Structural Design (Including Loads).

* Staff Scientist, Vehicle Dynamics & Control Group, Huntsville Research & Engineering Center. Member AIAA.

† Aerospace Engineer, Dynamics and Control Division, Aero-Astrodynamics Laboratory.

where $\tilde{F} = F - kG\bar{a}'$. Equations (8) and (9) have to be solved backward in time starting at T with the initial conditions $P(T) = 0$; $\xi(T) = 0$. Hence, for any given vehicle data $F(t)$, $G(t)$, $k(t)$, and weighting matrix Q, Eq. (8) can be solved. Knowing $P(t)$, the total wind profile $\alpha_w(t)$, and its effectiveness $H(t)$ allows one to solve Eq. (9) in a second step. Substitution of $P(t)$ and $\xi(t)$ into Eqs. (7) and (6) finally results in the desired optimal control law as a function of flight time, which is characterized by feedback of all state variables, feedforward of the wind angle of attack α_w and of an additional signal $G'\xi$ which again is a function of the disturbance α_w according to Eq. (6).

In order to illustrate the properties of such optimal controller designs, a numerical example is given which was computed for a large expendable Post-Saturn launch vehicle of 150-m length with first and second bending mode frequencies in the order of 0.35 and 0.9 Hz, respectively, which was aerodynamically unstable at all times.[1] A typical solution for an assumed wind disturbance peaking at 79 sec is shown in Fig. 1 for a simple rigid-body representation of the vehicle dynamics with the state variables $\bar{x}' = [\theta, \dot{\theta}, \dot{Z}/V]$. Optimization over the full ascent trajectory (0, 150 sec) results in the three optimal gain schedules of Fig. 2, curves A. The elements of ξ resemble the assumed wind profile $\alpha_w(t)$.

Effects of Reduced Optimization Interval

Efforts were made to reduce the computational load and the amount of a priori knowledge concerning disturbances by dividing the total mission time into a limited number of finite optimization intervals. The results are illustrated in Figs. 1 and 2. At a time of high wind loads at $t = 70$ sec, only 40 sec or 20 sec of the coming wind disturbance were assumed to be known a priori. Despite poor guesses concerning the new end conditions of the P-matrix which was assumed to be zero at the end points, 110 sec (case B) and 90 sec (case C), respectively, the Riccati solution approached the

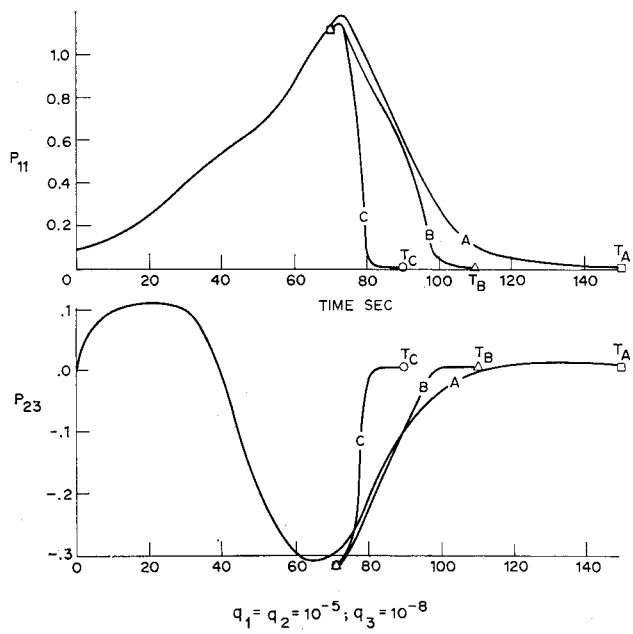

Fig. 1 Typical solutions of the matrix Riccati Eq. (8) for optimal control of a large expendable launch vehicle during atmospheric flight. (The two variables shown, P_{11} and P_{23}, are representative examples of the six elements of the symmetric 3 × 3-P-matrix.) Optimization interval reduced to (70, 110 sec) in case B and to (70, 90 sec) in case C.

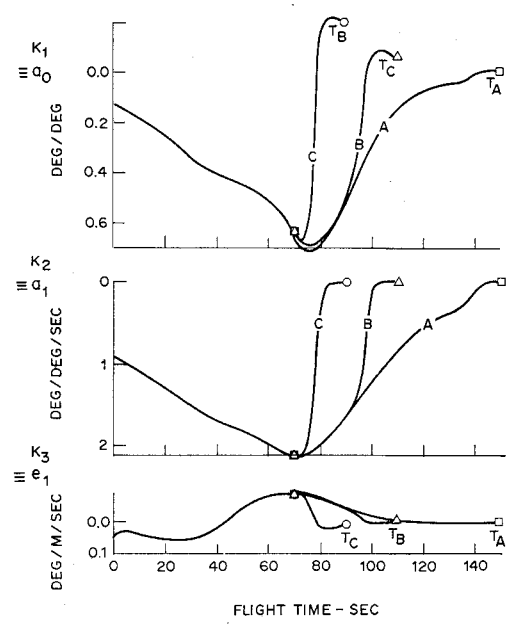

Fig. 2 Optimal feedback gains $K(t) = -G'P - k\bar{a}'$ computed via linear optimal control theory. Deviations from the optimal values due to reduced optimization intervals (curves B and C) are caused by the long transients of the Riccati solutions.

optimal solution of case A, computed over the essentially unlimited interval, in about 15 sec with less than 10% error. If this transient solution were used to compute optimal gain schedules, this would result in the curves B and C of Fig. 2. Thus in case C with an assumed 20 sec a priori knowledge of α_w (from 70 to 90 sec flight time) optimization theory would have yielded the feedback and feedforward gains to within 10% of the optimal values for the time interval 70 to 75 sec.

Although there are no theoretical results available at the present time concerning admissible reductions of the optimization time intervals in the case of external disturbances, the good agreement between infinite interval and finite interval optimization in a large number of numerical examples has led to the development of a practical optimization method based upon finite optimization intervals involving forward integrations only, as described next.

Floating Interval Optimization

For regulator design without specified terminal conditions the computational load can be greatly reduced if the total flight time is divided into a finite number of optimization intervals and if the mn gain schedules of $K(t)$ are assumed to be piecewise linear functions of time as shown in Fig. 3 (Ref. 2). Then the optimization problem is reduced to a sequence of parameter searches for the mn gain slopes $\dot{K}_j$ of

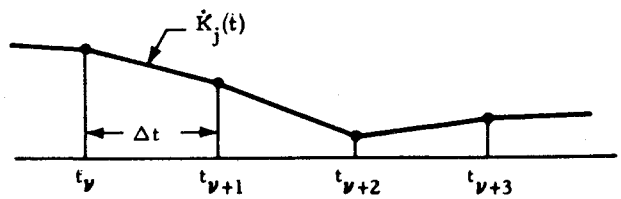

Fig. 3 Assumed polygonal form of optimal gain schedules.

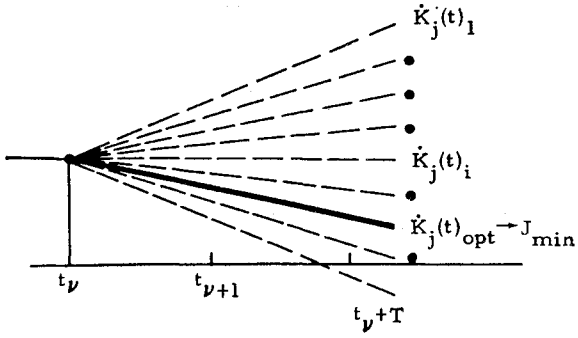

Fig. 4 During optimization cycle at time t_ν, a search is performed in $\dot{K}_j$ parameter space of the mn gain slopes for optimum performance.

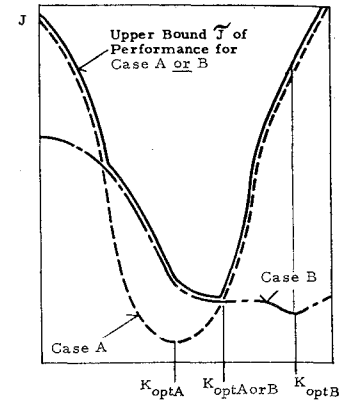

Fig. 5 Typical topology of performance index J as a function of scalar control parameter K considering possible occurrence of flight condition A or B.

the gain matrix $K(t)$ as shown in Fig. 4 which is performed over each of the optimization intervals.

In this regulator problem, the performance index does not contain the terminal state. Thus, forward integrations which can be performed efficiently on analog or hybrid computers are sufficient to determine the optimum. The dynamic simulation serves a dual purpose. Performance is repetitively evaluated during an optimization cycle in fast time. Once the optimum set of gain slopes $\dot{K}_j$ ($j = 1, 2, \ldots, mn$) is determined, the optimum parameters are used during a real-time simulation from one update time (t_ν) to the next ($t_{\nu+1}$) using the same dynamic model. After the last updating, the complete time history of the simulated optimum system is available for performance evaluation. This allows immediate decisions concerning refinement or redirection of the design effort to be made.

In order to distinguish between local minima and absolute minima, the search in the $\dot{K}_j$ parameter space is performed in two phases, a systematic grid search and a gradient search. In the systematic grid search, all possible parameter combinations within a region of specified limits and a grid of specified fineness are evaluated for their performance J. Such a complete survey is feasible as long as the parameter space is of low dimension as in present applications. In the gradient search, the Fletcher-Powell-Davidon gradient method[3] uses the grid search minimum as a starting point to precisely locate the minimum.

Mathematical Representation of Design Objectives

The present optimization technique offers the designer a wide selection of performance measures he can use to represent the design goals. Whereas the performance index J must be of a prescribed mathematical form (e.g., quadratic) in most classical optimization methods, the only requirement imposed on the performance measure in this technique is that J be a positive definite functional of the parameters to be optimally adjusted and of the vehicle state in the floating optimization interval $(t_\nu, t_\nu + T)$

$$J = J[K(\tau); \bar{x}(\tau)]; \; t_\nu \leq \tau \leq t_\nu + T \tag{10}$$

Although this restriction excludes trajectory optimization problems which depend mainly on terminal constraints, the technique is applicable to a wide class of regulator or control system optimization problems.

A shortcoming of all time-domain optimization techniques —the strong dependence of optimal solutions on specific flight and disturbance conditions—has been greatly reduced by the following approach. At least two adverse flight conditions (case A and case B) are repetitively simulated and analyzed for optimum performance. This results in two performance measures, $J_A(K, \bar{x})$, $J_B(K, \bar{x})$, for each set of parameters K in a given optimization interval as shown in Fig. 5 for a scalar control parameter K. The minimum of the upper bound $\tilde{J}$ represents the optimum adjustment in view of the uncertainty in flight conditions. Neither K_{optA} nor K_{optB} would be optimal in view of the uncertainty concerning the flight condition. Performance might be unacceptably poor if case A occurred and the control parameter K_{optB} were used. The best tradeoff in view of this uncertainty is the minimum of the upper bound $\tilde{J}$ of J_A and J_B (solid line in Fig. 3).

The minimization scheme will use the worse-case ($\tilde{J}$ in Fig. 5), in the search for new parameters which can be expressed in the form of a minimax problem:

$$J = \max J_i[K(\tau), \bar{x}(\tau)] \rightarrow \min \tag{11}$$

$$i = \text{Case A, Case B} \qquad t_\nu \leq \tau \leq t_\nu + T$$

The optimized gain schedules $K_j(t)$ will thus represent the best tradeoff in view of likely occurrence of either flight conditions A or B.

The most direct way to locate the minimum of the upper performance bound is to simulate all possible flight conditions for a given set of control parameters in order to determine the upper bound $\tilde{J}$. A gradient-dependent minimization technique can again be applied to seek the minimum. One might expect convergence difficulties around the corners of these $\tilde{J}$-functions. However, only minor modifications were necessary to the basic Fletcher-Powell-Davidon gradient scheme[3] and to the preceding grid search to locate corner-type minima. The changes included a relaxing of the gradient convergence test ($|\nabla J| \leq \varepsilon$, where ε is a small specified number). If all other convergence tests are passed, then ε is doubled in subsequent iterations.

First Example: Load Relief Pitch Controller Design for "Phase B" Space Shuttle

The atmospheric flight phase of a two-stage reusable space shuttle provides an excellent opportunity to apply and refine this computerized design tool. Since the technique is based on repetitive simulation of the complete flight dynamics, great care is required in describing the vehicle and flight path. The large aerodynamic forces of the winged space shuttle configurations as developed under recent phase B studies cause strong interactions between vehicle dynamics and flight path. In order to limit the complexity of the computer simulation, it is assumed that rigid-body perturbation equations about a nominal point-mass gravity-turn trajectory adequately describe the over-all dynamics. The requirement for trimmed flight along a specified trajectory leads to a set of trim equations which prescribe trim values for angle of

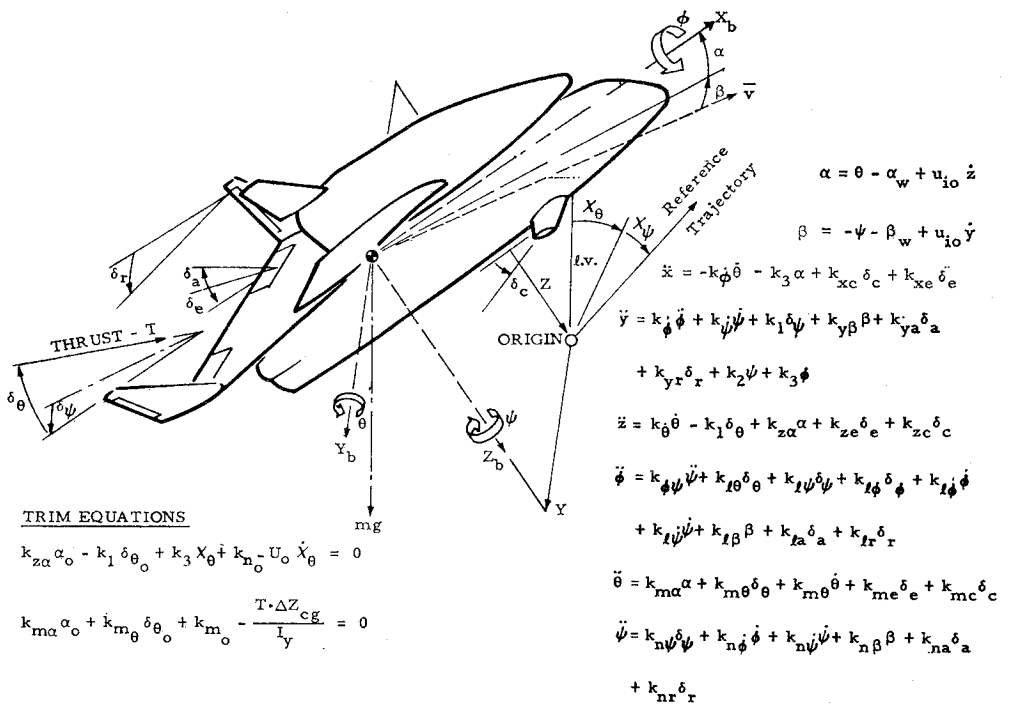

Fig. 6 Sign conventions, notations and 6-degree-of-freedom perturbation equations of motion for space shuttle ascent.

attack and engine gimbal angle. The coordinate system, major notations, and dynamic equations used are shown in Fig. 6 (Ref. 4).

In order to obtain a direct indication of control action related structural load reductions, it is necessary to compute representative loads during simulations. A simple form was adopted from previous (wingless) symmetrical booster control practice in the early phase of this study[5]

$$M_B(x) = M_\alpha(x) \cdot (\alpha_0 + \alpha) + M_{\delta\theta}(x) \cdot (\delta_{\theta_0} + \delta_\theta). \quad (12)$$

Since aerodynamic load distributions (required to determine these bending moment partials) were not readily available, loads were indicated in a form less dependent on aerodynamic distribution as suggested in[6]

$$\text{Bending Moment Indicator} = M_B(x)/M_\delta(x)$$

$$= R(x)(\alpha_0 + \alpha) + \delta_0 + \delta \quad (13)$$

where

$$R(x) = M_\alpha(x)/M_\delta(x) \quad (14)$$

Based on approximate load distributions, $R(x)$ was calculated for the booster-orbiter rear attachment point for the configuration studied.

Since reduction of peak loads is of major concern to the designer, the most direct approach to accomplish this was to express the performance index in terms of the peak bending loads encountered in each simulation

$$J = \max|M_B(\tau)/M_\delta| \rightarrow \min; \qquad t_v \leq \tau \leq t_v + T \quad (15)$$

An additional term had to be included to limit sudden vehicle rotations in response to high wind shears and thus assure a sufficient amount of trajectory stability. A simple, yet effective, stability term is

$$J_s = \int_{t_v}^{t_v+T} |\dot{\theta}|\,dt \quad (16)$$

which was added to the basic load relief criterion [Eq. (15)]. The complete load relief performance index which accounts for likely occurrence of either one of two adverse wind conditions then becomes

$$J = \max_{\substack{i=\text{Wind } A,\\ \text{Wind } B}} \left\{ \max|M_B(\tau)/M_\delta'| + q \int_{\substack{t_v \\ \leq t_v\tau \leq t_v+T}}^{t_v+T} |\dot{\theta}|\,d \right\}_i \quad (17)$$

This criterion was applied to determine load relief control gain schedules for the space shuttle configuration described in Ref. 7.

Two synthetic head wind profiles from Ref. 8 were used to represent adverse flight conditions and thus reduce the sensitivity of the optimal controller to off-nominal wind conditions.

Typical results are shown in Fig. 7 where loads and dynamic response of the optimized system are compared with a conventional constant gain controller. A simple attitude error plus rate error feedback law was used in both cases

$$\delta_\theta(s) = -15(a_0 + a_1 s)\theta(s)/(s + 15). \quad (18)$$

The floating optimization interval was 15 sec. However, the optimization of gain slopes a_0, a_1 was updated every 5 sec as indicated by the break points in the optimal gain schedules. A drastic 50% load reduction is achieved for the more severe disturbance A, whereas loads in the less critical case B are only slightly reduced by 13%. A near-perfect tradeoff between the two likely disturbance cases is indicated by almost identical peak loads

$$J_{A\max} \approx J_{B\max} = 0.39 \quad (19)$$

A surprising feature of these optimal gain schedules is the sign reversal of the attitude error gain schedules $a_{0\theta}t(t)$ in the high dynamic pressure region resulting in positive feedback of attitude errors. A detailed analysis reveals that structural loads are substantially reduced if the vehicle's natural rotation into the wind ($\theta < 0$) due to its inherent weathercock stability is increased by the control system from a $\theta = -2°$ peak in the constant gain case to a peak value of $-3°$ in the optimized flight. Total engine deflections $\delta_\theta + \delta_{\theta o}$ in this load-critical flight region are dominated by trim requirements $\delta_{\theta o}$ which call for large positive trim deflections up to 6° at $t = 60$ sec. The constant gain controller further increases engine deflections to more than 8° whereas the negative attitude gains

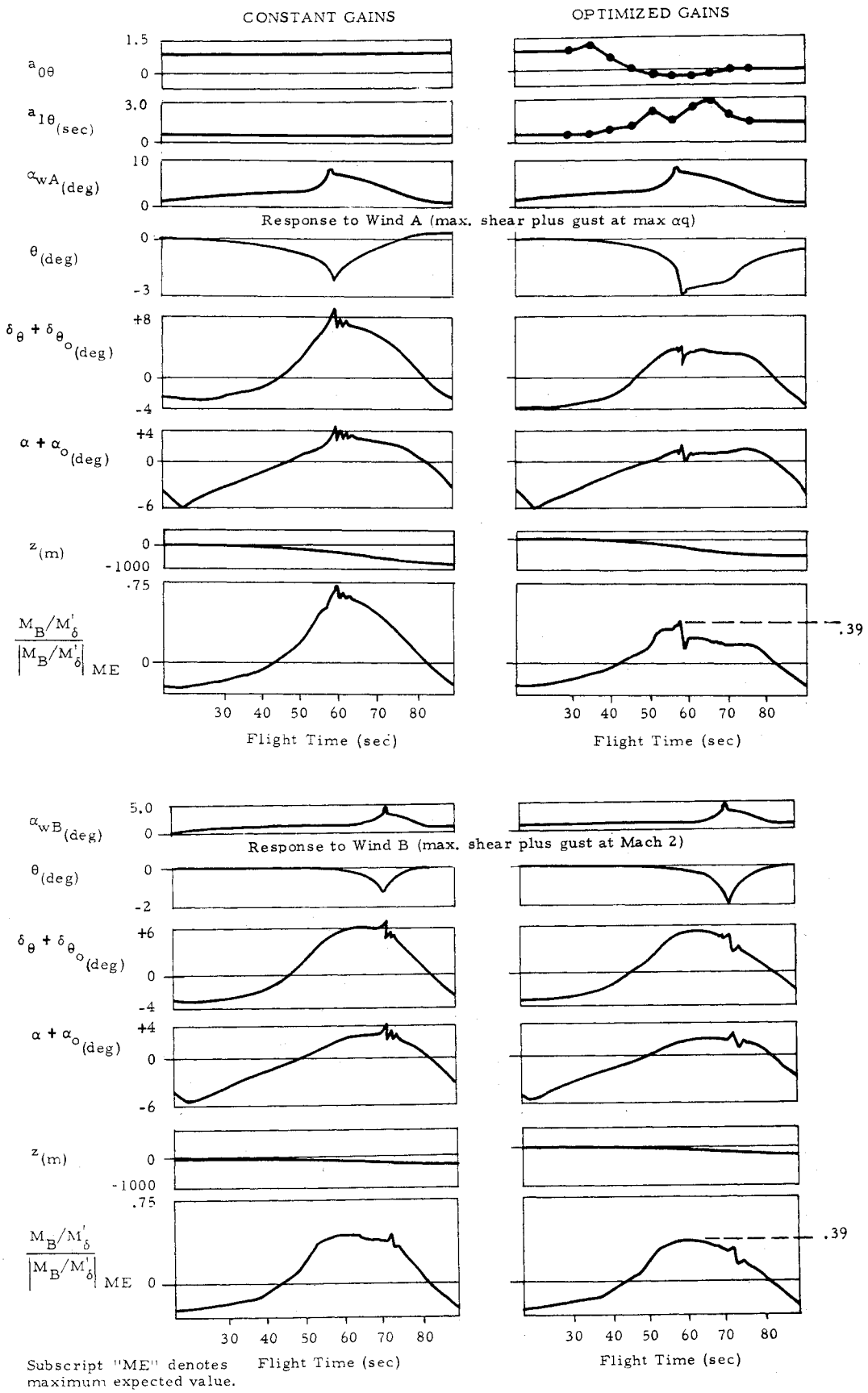

Fig. 7 Pitch control gain optimization for maximum load relief for a "phase-B" space shuttle configuration[7] using performance criterion Eq. (17) with floating optimization interval $T = 15$ sec and stability weighting factor $q = 0.75$. Design is based on two different wind profiles (A and B). Constant gain control system response is shown for comparison.

Table 1 Comparison of major performance characteristics for varying weighting factor q in performance index Eq. (17)

q	$\theta_{\max}$	$\delta_{\max}$	z at $t = 100$ sec	$\frac{M_{B\max}}{M_{BME}}$	Remarks
0.75	−8.0°	6.7°	−380 m	−0.62	Load minimum
0.96	−7.5°	7.2°	0	−0.63	Drift minimum
1.5	−5.0°	9.4°	+400 m	−0.85	Minimum attitude error

$a_{0\theta}$ of the optimized system reduce total deflections to about 4°. Since total deflections $\delta_\theta + \delta_{\theta 0}$ remain positive throughout the region of high headwind loads, vehicle stability is maintained in spite of the temporary positive feedback signal $a_{0\theta}$.

The computations were carried out on an EA1 8900 hybrid computer. A compressed time scale of 1000 times real time for the repetitive simulations resulted in approximately 5 min over-all computing time, including real-time simulation and recording of optimal performance. A few preliminary runs were necessary to establish a satisfactory weighting factor q which assures admissible trajectory deviations. The ease and effectiveness in shaping vehicle performance to the designer's needs by proper adjustment of the single weighting factor q is evidenced in Table 1, where three optimization results for an earlier shuttle configuration are compared; they were obtained by varying the weighting factor q in Eq. (17) from 0.75 to 1.5. For low q the load relief term dominates J causing low peak loads but large attitude errors and drifting with the wind, whereas high weighting of the intergal term in Eq. (17) results in small attitude error, larger structual loads, and upwind drift. With little effort a weighting factor adjustment $q = 0.96$ was found that minimized terminal drift for the two wind cases considered.

Second Example: Maximum Payload Yaw Controller Design for "Phase B" Space Shuttle

For the computerized design of a payload-optimal ascent control system it is necessary to derive payload sensitivities of all flight characteristics affected by attitude control dynamics.

The following performance index comprises the major payload penalties which depend upon flight control system performance

$$J' = \sum_{i=1}^{6} \frac{\partial P}{\partial R_i}(|R_i|_{\max} - R_{i0}) + \sum_{j}^{3} \frac{\partial P}{\partial \delta_j}(|\delta_j|_{\max} - \delta_{j0}) + \sum_{m=1}^{3}\left(\frac{\partial P}{\partial x_m} x_m(t_g) + \frac{\partial P}{\partial v_m} v_m(t_g)\right) \quad (20)$$

where P = payload penalty or decrease; R_i = forces at the booster-orbiter interface; δ_i = main booster engine gimbal angles for roll, pitch, yaw control including δ_{trim}; x_m = deviations from reference trajectory in x, y, z direction; v_m = velocity errors with respect to reference trajectory in x, y, z direction; t_g = start of closed-loop guidance phase, end of atmospheric disturbances. The subscript 0 denotes minimum design values specified by constraints not related to ascent.

The design goal of maximum payload can then be achieved by minimization of this payload penalty functional J'.

One of the space shuttle configurations from recent phase B studies was chosen to verify the concept of payload-optimal control system design.[7] The dynamic equations used in the hybrid simulation had to be expanded, however, to provide "in-flight" information about all the variables which affect the performance index J' of Eq. (20). The approach used in deriving the various payload sensitivity terms will be briefly discussed in the following sections.

Structural load impact on payload

Booster dry weight is strongly dependent on peak structural loads encountered during powered ascent. The standard practice of bending moment calculations proportional to angle of attack and engine deflection as used for symmetrical boosters and for pitch control studies of winged unsymmetrical boosters fail to adequately describe structural loads in three dimensions for general 6-DOF vehicle motion stabilized by a three-axis attitude control system.

Analyses of structural load concentrations in the composite two-stage shuttle vehicle revealed that the interface loads acting between booster and (piggy-back mounted) orbiter at the attachment points indicate with sufficient accuracy peak booster fuselage loads and related structural weight requirements.

Knowing the motion of the composite vehicle $(\vec{U}, \vec{\Omega})$ from the 6-D ascent simulation the interface forces and moments (subscript I) can be determined as part of the total external forces acting on the orbiter (subscript Or) which lead to the orbiter's known motion $\vec{U}, \vec{\Omega}$

$$\begin{aligned} \vec{F}_I &= m_{Or}(\dot{\vec{U}} + \vec{\Omega} \times \vec{U}) - \vec{F}_{aOr} - \vec{F}_{cgOr} - m_{Or}\vec{g} \\ \vec{M}_I &= [I_{Or}]\dot{\vec{\Omega}} + \vec{\Omega} \times [I_{Or}]\vec{\Omega} - \vec{M}_{aOr} \end{aligned} \quad (21)$$

where subscript a denotes aerodynamic effect, $\vec{F}_{CG}$ is the centrifugal force due to the orbiter's CG offset $\vec{r}_{CG}$ from that of the composite vehicle and $[I_{Or}]$ is the orbiter's moment of inertia matrix. Based on the given design of the booster-orbiter attachment points as shown in Fig. 8, the interface forces can be computed during simulations as functions of known quantities or simulated variables

$$\vec{R} = f(\vec{U}, \dot{\vec{U}}, \vec{\Omega}, \dot{\vec{\Omega}}, \vec{F}_{aOr}, r_{CG}). \quad (22)$$

In the shuttle configuration studied, $\vec{R}$ is a six-dimensional vector of force components.

A structural analysis of the booster fuselage in the region of the orbiter attachment points revealed that the peak interface forces R_{2z}, R_{3z}, R_{4y} strongly affect the booster hydrogen tank design. The hydrogen tank is compression-critical rather than pressure-critical.[9] The stress resultant N_x in the axial direction determines the design. In the first approximation, no circumferential variation was considered and N_x was determined by summing the effects of axial compression and bending from a one-dimensional internal load analysis. Given the maximum compressive loads, the stiffeners of each barrel can be designed by using the formulation given in Ref. 10. The simultaneous occurrence of general instability, skin buckling,

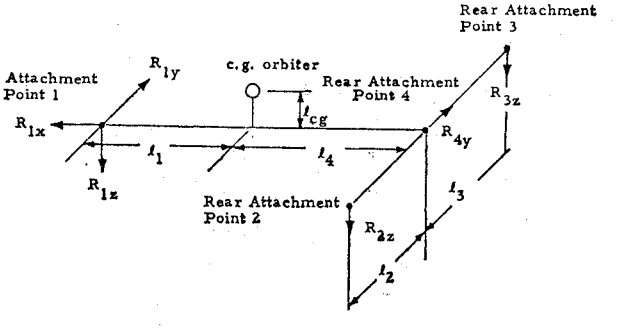

Fig. 8 Components of interface forces and geometry of the attachment points of shuttle booster and orbiter.[7]

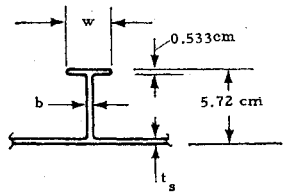

Fig. 9 Cross section of booster hydrogen tank stiffener rings; b, t_s, w are varied according to peak load distribution.

and web crippling determines the design point; i.e., the dimensions w, b, and t_s of the tank stiffeners in Fig. 9.

In order to account for general unsymmetrical loads, the total force at the three rear attachment points 2, 3, and 4

$$R_r = [(R_{2z} + R_{3z})^2 + R_{4y}{}^2]^{1/2} \tag{23}$$

must be computed. Peak values of R_r can then be used to determine the booster's H_2-tank weight. The mass sensitivity of the booster H_2-tank for changes in interface load R_r is then found to be

$$\Delta W_{H_2(\text{Tank})}/\Delta R_r = 0.0104 \text{ kg/N}$$

which can be expressed in a payload penalty ΔP according to Ref. 11

$$\frac{\partial P}{\partial R_r} \approx \frac{\Delta P}{\Delta R_r} = \frac{\Delta W_{H_2(\text{Tank})}}{\Delta R_r} \frac{\Delta P}{\Delta W_{\text{Booster}}} = 0.0104 * 0.3 = 0.00208 \frac{\text{kg}}{\text{N}}$$

Since the tank c.g. is only 0.6 m from the booster c.g. upon burnout, no additional penalty due to hypersonic trim requirements is necessary.

Impact of engine gimbal angle requirements on payload

The major effects of maximum engine gimbal angles on space shuttle payload were determined in a recent study.[12] An increase in engine deflection δ requires a heavier actuator system, larger engine base area with associated increase in drag, structural weight and fuel requirement. Typical values for the payload penalty $\partial P/\partial\delta$ were found in Ref. 11 to be of the order

$$\partial P/\partial\delta = 221 \text{ kg/deg}$$

This value was also used in the present study for all total gimbal angles $\delta_{\text{Trim}} + \delta$ which exceed the nominal design values.

Impact of trajectory deviations on payload

Vehicle insertion weight variations produced by trajectory deviations were asssumed to be a function of the vehicle state at the start of active closed-loop guidance at $t_g = 100$ sec into ascent when atmospheric disturbances have virtually died out. These trajectory-related penalty functions were computed using a trajectory computation program incorporating a quasi-optimal guidance concept. Insertion weight deviations were computed for each parameter of the vehicle state taken singly. Coupling terms were neglected to simplify the analysis. It was planned to include coupling effects later if a significant payload impact of trajectory errors should result from the early studies. The insertion weight was initially expressed by a quadratic function of the form.

$$\Delta W_{\text{ins}} = \sum_{m=1}^{3} \left[\frac{\partial W}{\partial x_m} x_m(t_g) + \frac{\partial W}{\partial v_m} v_m(t_g) + \frac{\partial W}{\partial x_m{}^2} x_m{}^2(t_g) + \frac{\partial W}{\partial v_m{}^2} v_m{}^2(t_g) \right] \tag{24}$$

For this particular zero-lift trajectory the quadratic terms were found to be two or more orders of magnitude smaller than the linear terms and were therefore neglected. The following payload penalty coefficients were calculated in second stage burn time and converted to payload penalty based on Ref. 11 for use in performance criterion [Eq. (20)]

$$\frac{\partial P}{x(100 \text{ sec})} = -0.061 \frac{\text{kg}}{\text{m}}; \qquad \frac{\partial P}{|y(100 \text{ sec})|} = 0.027 \frac{\text{kg}}{\text{m}}$$

$$\frac{\partial P}{z(100 \text{ sec})} = 0.035 \frac{\text{kg}}{\text{m}}; \qquad \frac{\partial P}{\dot{x}(100 \text{ sec})} = -6.8 \frac{\text{kg}}{\text{m/sec}}$$

$$\frac{\partial P}{|\dot{y}(100 \text{ sec})|} = 0.43 \frac{\text{kg}}{\text{m/sec}}; \qquad \frac{\partial P}{\dot{z}(100 \text{ sec})} = 4.0 \frac{\text{kg}}{\text{m/sec}}$$

In order to avoid excessive angular rates and side slip angles β by the vehicle in response to gust-type wind disturbances, an additional cost functional was formulated:

$$J'' = \frac{1}{T} \int_{t_v}^{t_v+T} [|\beta| + q_\psi |\dot{\psi}| + q_\phi |\dot{\phi}|] dt \tag{25}$$

where $\dot{\phi}$ and $\dot{\psi}$ are the roll and yaw rates, respectively. $q_{\dot{\psi}}$ and $q_{\dot{\phi}}$ are weighting coefficients reflecting the design constraints imposed on side slip and vehicle rates. J'' should be kept small to assure smooth flying qualities. The criteria J' and J'' can be readily combined into a single performance criterion

$$J = J' + qJ'' \rightarrow \min \tag{26}$$

which makes possible the minimization of all payload penalties while a weighted flying quality criterion qJ'' is simultaneously satisfied.

All three weighting factors (q, $q_{\dot{\phi}}$, $q_{\dot{\psi}}$) can be readily related to specified design guidelines concerning admissible angular rates and side slip angles. They are therefore easy to adjust after a small number of trial optimizations. This is a major advantage over quadratic form J functionals where a large number of weighting factors must be selected for this high-order problem.

Optimization Results

The yaw and roll thrust vector control laws were of the following form

$$\delta_\psi = a_{0\psi}\psi + a_{1\psi}\dot{\psi} - b_{0\psi}\beta, \qquad \delta_\phi = a_{0\phi}\phi + a_{1\phi}\dot{\phi} \tag{27}$$

Actuator dynamics were assumed to be identical to the pitch control system [Eq. (18)]. Typical results of an optimization of gain schedules for yaw error feedback $a_{0\psi}(t)$ and side slip angle feedback $b_{0\psi}(t)$ are presented in Fig. 10 and compared with a constant gain system. Again the vehicle was subjected to two different wind profiles, a sidewind A (solid lines, maximum shear plus superimposed gust at 58 sec) and a sidewind B (dashed lines, maximum shear plus gust at 75 sec) acting 90° from the right. Payload penalties in the performance criterion (30) were dominated by the structural weight contributions

$$\Delta P_R = \sum \left(\frac{\partial P}{\partial R_i} \left| Ri \right|_{\max} - R_{i0} \right)$$

recorded in the bottom strip of Fig. 10. The impact of gimbal angle requirements above the nominal design limit ($\delta_0 = 7°$) was generally less than 15% of ΔP_R and trajectory-related penalties were another order of magnitude smaller and therefore not recorded. A major design objective was to limit roll (ϕ) and sideslip (β) excursions as enforced by high weighting factors q, $q_{\dot{\phi}}$, and $q_{\dot{\psi}}$ in performance index (26). The resulting gain schedules drive yaw error feedback to zero and sideslip feedback to high values in the max q region, thus reducing sideslip from over 5° to approximately 1° by yawing the vehicle into the wind. At the same time the payload penalty ΔP_R is reduced by 1800 kg for the worst sidewind case A.

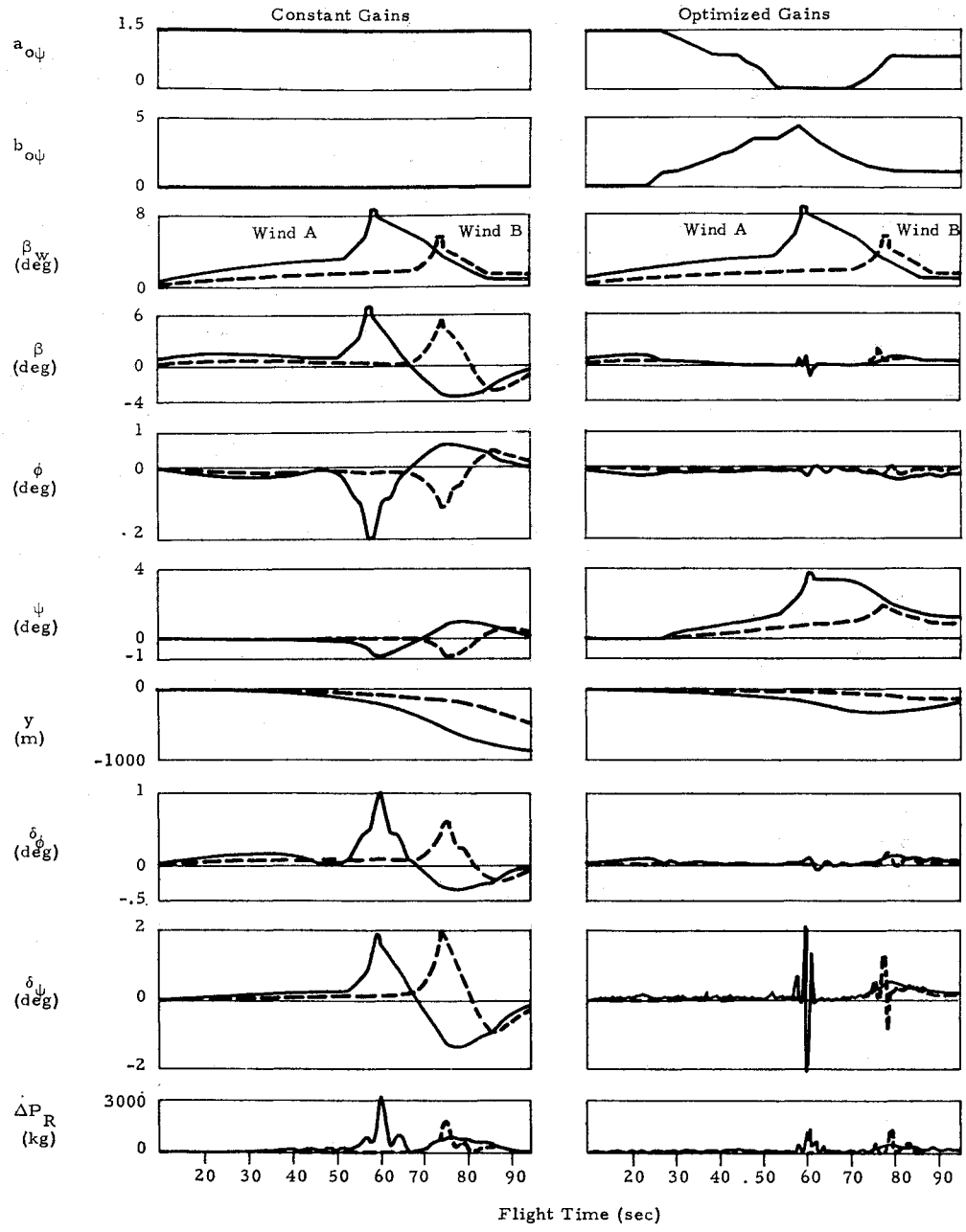

Fig. 10 Optimization of yaw control gains for maximum payload as expressed in performance criterion Eq. (26) for a "phase-B" space shuttle.[7] Design is based on two different sidewind cases (A, B). Constant gain control system response is shown for comparison.

Again a good tradeoff between the two wind cases is achieved: Both sideslip angle β and payload penalty ΔP_R show similar peak values for the optimized controller which is an indication for low sensitivity of the optimal control system to wind uncertainties.

The optimization technique has been successfully extended to include aerodynamic control to augment main engine thrust vector control in a "payload-optimal" manner. To this end the hinge moment increases caused by aileron or elevon deflections are related to wing weight increases and a corresponding payload penalty term is included in the performance index.

Conclusions

The restriction to piecewise linear time functions for the optimized control gain schedules and to regulator-type control problems where performance is governed by the current or near-future state has led to a sequential hybrid computer optimization technique. Repetitive forward integrations of the complete dynamic system, most efficiently performed by hybrid computer, are combined with a gradient minimization scheme. In this approach the performance index can include the effects of attitude control on structural weight and other weight penalties which depend upon the control system. Valuable insight concerning the interactions between attitude control, structural loads, structural weight, and trajectory performance can be gained at an early design phase.

In the first example, the pitch controller design for the ascent of a "Phase B" space shuttle configuration, the design objective was minimization of peak structural loads. Contrary to conventional load relief practice the optimization scheme led to gain schedules with positive attitude feedback in the max-q flight region. Trim requirements for the selected trajectory together with the high aerodynamic stability in pitch maintain vehicle stability in spite of this destabilizing attitude feedback. In the second example the design goal expressed in the performance index was minimization of all weight penalties affected by the attitude control system. In the numerical example structural weight penalties dominated strongly the performance measure. The resulting yaw controller exercised tight control over side slip by causing the

vehicle to yaw into the sidewind. This in turn reduced roll errors and structural weight.

The sensitivity of the optimized control system to wind uncertainties has been reduced by using more than one wind profile during the optimization. The realism of hybrid simulation of the complete vehicle dynamics including nonlinearities, the freedom in formulating the design objectives and the reduced sensitivity of the optimal solution to disturbance uncertainties make this approach a practical engineering tool.

References

[1] Trautwein, W. and Tuck, J. G., "Control System Optimization for Saturn V Launch Vehicles Using Gradient Techniques," Final Report, LMSC-HREC A791836, Oct. 1968, Lockheed Missiles & Space Co., Huntsville, Ala.

[2] Trautwein, W. and Connor, C. L., "Hybrid Computer Solutions for Optimal Control of Time-Varying Systems with Parameter Uncertainties," *Proceedings, Fall Joint Computer Conference*, Houston, Texas, 1970, pp. 135–142.

[3] Fletcher, R. and Powell, M. J. D., "A Rapidly Convergent Descent Method for Minimization," *Computer Journal*, Vol. 6, 1963, pp. 163–168.

[4] Connor, C. L. and Trautwein, W., "Application of Optimal Control Techniques to Advanced Manned Missions," Final Report, LMSC-HREC D225541, Feb. 1972, Lockheed Missiles & Space Co., Huntsville, Ala.

[5] Livingston, J. M., Jr., and Redus, J. R., "Load-Reducing Flight Control Systems for the Saturn V with Various Payloads," AIAA Paper 68-843, Pasadena, Calif., 1968.

[6] Ryan, R. S. and Mowery, D. K., "A Look at Control Law Influences on the Rigid Body Bending Moments for Boost Vehicles with Various Degrees of Aerodynamic Stability," AIAA Paper 71-918, Palo Alto, Calif., 1971.

[7] "Space Shuttle Program Phase B Final Report—Technical Summary," Rept. MDC E0308, Part II, March 15, 1971, McDonnell Douglas Corp., St. Louis, Mo.

[8] Daniels, G. E., ed., "Terrestrial Environment (Climatic) Criteria Guidlines for Use in Space Vehicle Development, 1969 Revision," TM X-53872, 1970, NASA–MSFC.

[9] Anderson, H. A., "Booster Hydrogen Tank Cylinder Design," Design Note B-WEST-STR-3, Sept. 1970, McDonnell Douglas Corp., St. Louis, Mo.

[10] Wright, F. M., "Minimum Weight Design of Flanged Isogrid Cylinders in Compression," Design Note, B-WEST-STR-7, Sept. 1970, McDonnell Douglas Corp., St. Louis, Mo.

[11] Garrison, G. S. and Kilpatrick, D. R., "Shuttle Exchange Ratio Study Using the McDonnell Douglas High Crossrange Canard Configuration 20," M-796-945, May, 1971, Northrop Corp., Huntsville, Ala.

[12] Ryan, R. S., Baccus, D. L., Hall, C. E., and Mowery, D. K., "Space Shuttle Engine Gimbal Requirements," Marshall Space Flight Center, Jan. 1971, Aero-Astrodynamics Lab., Huntsville, Ala.